

# Ultrashort Echo Time for Improved Positive-Contrast Manganese-Enhanced MRI of Cancer

Joris Tchouala Nofiele<sup>1,2</sup>, Hai-Ling Margaret Cheng<sup>1,2\*</sup>

**1** Department of Medical Biophysics, University of Toronto, Toronto, Canada, **2** The Research Institute and Diagnostic Imaging, The Hospital for Sick Children, Toronto, Canada

## Abstract

**Objective:** Manganese (Mn) is a positive magnetic resonance imaging (MRI) contrast agent that has been used to obtain physiological, biochemical, and molecular biological information. There is great interest to broaden its applications, but a major challenge is to increase detection sensitivity. Another challenge is distinguishing regions of Mn-related signal enhancement from background tissue with inherently similar contrast. To overcome these limitations, this study investigates the use of ultrashort echo time (UTE) and subtraction UTE (SubUTE) imaging for more sensitive and specific determination of Mn accumulation.

**Materials and Methods:** Simulations were performed to investigate the feasibility of UTE and SubUTE for Mn-enhanced MRI and to optimize imaging parameters. Phantoms containing aqueous Mn solutions were imaged on a MRI scanner to validate simulations predictions. Breast cancer cells that are very aggressive (MDA-MB-231 and a more aggressive variant LM2) and a less aggressive cell line (MCF7) were labeled with Mn and imaged on MRI. All imaging was performed on a 3 Tesla scanner and compared UTE and SubUTE against conventional  $T_1$ -weighted spoiled gradient echo (SPGR) imaging.

**Results:** Simulations and phantom imaging demonstrated that UTE and SubUTE provided sustained and linearly increasing positive contrast over a wide range of Mn concentrations, whereas conventional SPGR displayed signal plateau and eventual decrease. Higher flip angles are optimal for imaging higher Mn concentrations. Breast cancer cell imaging demonstrated that UTE and SubUTE provided high sensitivity, with SubUTE providing background suppression for improved specificity and eliminating the need for a pre-contrast baseline image. The SubUTE sequence allowed the best distinction of aggressive breast cancer cells.

**Conclusions:** UTE and SubUTE allow more sensitive and specific positive-contrast detection of Mn enhancement. This imaging capability can potentially open many new doors for Mn-enhanced MRI in vascular, cellular, and molecular imaging.

**Citation:** Nofiele JT, Cheng H-LM (2013) Ultrashort Echo Time for Improved Positive-Contrast Manganese-Enhanced MRI of Cancer. PLoS ONE 8(3): e58617. doi:10.1371/journal.pone.0058617

**Editor:** Tone Frost Bathen, The Norwegian University of Science and Technology (NTNU), Norway

**Received:** November 6, 2012; **Accepted:** February 5, 2013; **Published:** March 4, 2013

**Copyright:** © 2013 Nofiele, Cheng. This is an open-access article distributed under the terms of the Creative Commons Attribution License, which permits unrestricted use, distribution, and reproduction in any medium, provided the original author and source are credited.

**Funding:** This study was supported by funding from The SickKids Foundation and The Garron Family Cancer Centre Small Grant Competition. The funders had no role in study design, data collection and analysis, decision to publish, or preparation of the manuscript.

**Competing Interests:** The authors have declared that no competing interests exist.

\* E-mail: Hai-Ling.Cheng@sickkids.ca

## Introduction

Manganese (Mn), an essential metal for our body, is one of the earliest reported paramagnetic contrast agents for magnetic resonance imaging (MRI) due to its efficient positive contrast enhancement [1,2]. Unlike gadolinium, a paramagnetic lanthanide ion approved for clinical use, manganese is an endogenous constituent and behaves like a calcium ion analogue that often acts as a regulatory cofactor in a number of important enzymes and receptors [3]. Its unique biological properties have lent themselves to various applications in functional and molecular imaging, most notably in imaging the liver [4], brain function [5], myocardial viability [6], and, more recently, cancer cells [7,8]. In virtually all applications, the standard protocol is a  $T_1$ -weighted pulse sequence to obtain positive signal contrast in areas of Mn accumulation.

One challenge to broadening the application of Mn-enhanced MRI is the need to increase detection sensitivity. Another

challenge is to distinguish regions of positive contrast due to Mn accumulation from other tissues with inherently similar signal intensity. This is a dilemma in any kind of contrast-enhanced imaging, and the convention of using a pre-contrast image for comparison is, in many cases, impractical, especially when contrast accumulation occurs slowly and image misregistration becomes an issue. A method that does not require pre-contrast imaging and permits specific yet sensitive determination of contrast accumulation is desirable.

Ultrashort echo time (UTE) pulse sequences [9] have been applied to negative contrast iron oxide nanoparticles for this precise purpose: to improve detection sensitivity and specificity [10,11]. In contrast to conventional “long” echo time sequences, UTE acquires signal very soon after excitation. This is particularly relevant to iron oxides, as it minimizes  $T_2$ - and  $T_2^*$ -related signal decay and reaps  $T_1$ -related signal enhancement, thereby turning the conventional “dark” contrast iron oxide into a “bright” contrast agent. Another unique feature of UTE is the capability to

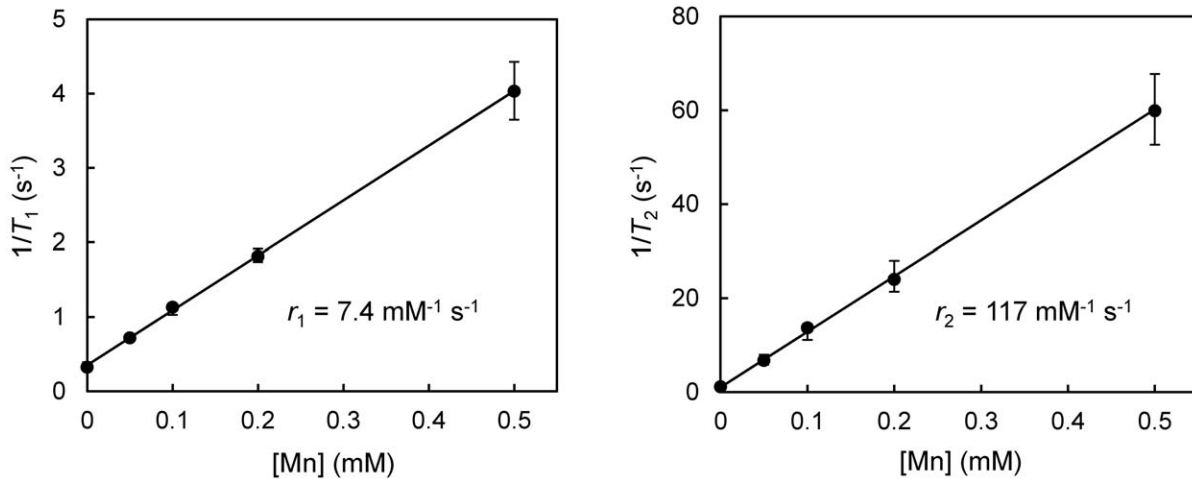


**Figure 1. Relaxivity measurements of MnCl<sub>2</sub> at 3 Tesla.** Relaxation rates  $1/T_1$  and  $1/T_2$  versus MnCl<sub>2</sub> concentration. Shown are mean values and standard deviations in each region-of-interest. Relaxivities  $r_1$  and  $r_2$  are calculated from linear regression slopes ( $R^2 = 0.9997$  for  $r_1$ ;  $R^2 = 0.9995$  for  $r_2$ ). doi:10.1371/journal.pone.0058617.g001

combine  $T_1$  and  $T_2^*$  effects synergistically by subtracting later echoes from the UTE image, thereby forming a subtraction UTE (SubUTE) image. In doing so, the  $T_2^*$ -related signal decay at the later echo is effectively reversed and added to the  $T_1$ -related signal increase on the UTE image. This subtraction method not only enhances sensitivity but also provides background suppression, since only areas of contrast agent accumulation would experience large  $T_1$  and  $T_2^*$  effects. The handful of investigations into UTE has demonstrated its utility for more specific and sensitive imaging [10,12], but these have focused primarily on negative-contrast iron oxides. The utility of UTE for imaging other MRI contrast agents remains largely unexplored.

In this study, our aim was to investigate the application of UTE and SubUTE to achieve more specific and sensitive positive-contrast detection of Mn enhancement. Although Mn is a  $T_1$ -enhancing agent and does not suffer from the same issues as negative-contrast iron oxides, it stands to benefit from more specific and sensitive detection. Amongst paramagnetic contrast agents, Mn may be uniquely suited to benefit from the synergistic  $T_1$  and  $T_2^*$  effects of SubUTE imaging, owing to a relatively large effect on the transverse relaxation rate. This study investigates the feasibility and optimization of UTE and SubUTE detection of Mn through theoretical and phantom studies. A proof-of-concept study is demonstrated for Mn-enhanced cancer imaging, showing that UTE imaging provides sensitive detection of aggressive breast cancers, with SubUTE providing the best specificity.

## Materials and Methods

### Theoretical Studies

The UTE sequence is a spoiled gradient echo (SPGR) acquisition where signal intensity is described by the following steady-state equation:

$$S = S_o \sin \theta \left( \frac{1 - e^{-TR/T_1}}{1 - e^{-TR/T_1} \cos \theta} \right) e^{-TE/T_2^*} \quad (1)$$

where repetition time (TR), echo time (TE), and flip angle ( $\theta$ ) are adjustable imaging parameters;  $S_o$  is a global sensitivity factor; and  $T_1$  and  $T_2^*$  are longitudinal and effective transverse magnetization relaxation times specific to the tissue. The UTE signal can be

modeled by setting TE to zero, thereby creating a purely  $T_1$ -weighted image with no  $T_2^*$ -related signal decay. If an image acquired at a later echo time is subtracted from the UTE image, i.e.  $\text{SubUTE}(TE) = S(\text{UTE}) - S(TE)$ , the resulting difference image provides synergistic  $T_1$  and  $T_2^*$  contrast.

In the presence of a MRI contrast agent such as Mn,  $T_1$  and  $T_2^*$  are approximated by:

$$\frac{1}{T_1} = \frac{1}{T_{1o}} + r_1[CA] \quad \frac{1}{T_2^*} = \frac{1}{T_{2o}^*} + r_2^*[CA]. \quad (2)$$

where the subscript 'o' denotes baseline (i.e. no contrast agent),  $r_1$  and  $r_2^*$  are contrast agent relaxivities, and [CA] is contrast agent concentration. Contrast, or the signal difference induced by these  $T_1$  and  $T_2^*$  changes, can be determined from Eqs. [1] and [2] as follows:

$$C = \Delta S = S_{[CA]} - S_{[CA]=0} \quad (3)$$

Contrast was evaluated for UTE imaging using a very short TE, using a longer TE typical in conventional SPGR imaging, and using SubUTE. Optimal settings for TR, TE, and  $\theta$  were investigated for various tissues with different baseline  $T_{1o}$  and  $T_{2o}^*$  relaxation times. This was accomplished by varying TR (6–100 ms), UTE (8–150  $\mu$ s), long TE (0.01–100 ms),  $T_{1o}$  (300–3000 ms),  $T_{2o}^*$  (25–100 ms) to assess a range of Mn concentrations (0.001–10 mM).

### Phantom Studies

Manganese chloride (MnCl<sub>2</sub>) solutions were prepared by dissolving manganese (II) chloride tetrahydrate (Sigma-Aldrich Canada Inc., Oakville, ON, Canada) in water at various concentrations. The solutions were placed in borosilicate glass tubes with a diameter of 6 mm and height of 50 mm. The phantoms were imaged on a 3 Tesla MRI scanner (Achieva 3.0T TX, Philips Medical Systems, Best, The Netherlands) using a 32-channel receive-only head coil. The  $r_1$  and  $r_2$  relaxivities of MnCl<sub>2</sub> were determined by measuring  $T_1$  and  $T_2$  relaxation times at different MnCl<sub>2</sub> concentrations and calculating the regression slope.  $T_1$  was measured using a 2D inversion-recovery turbo spin-

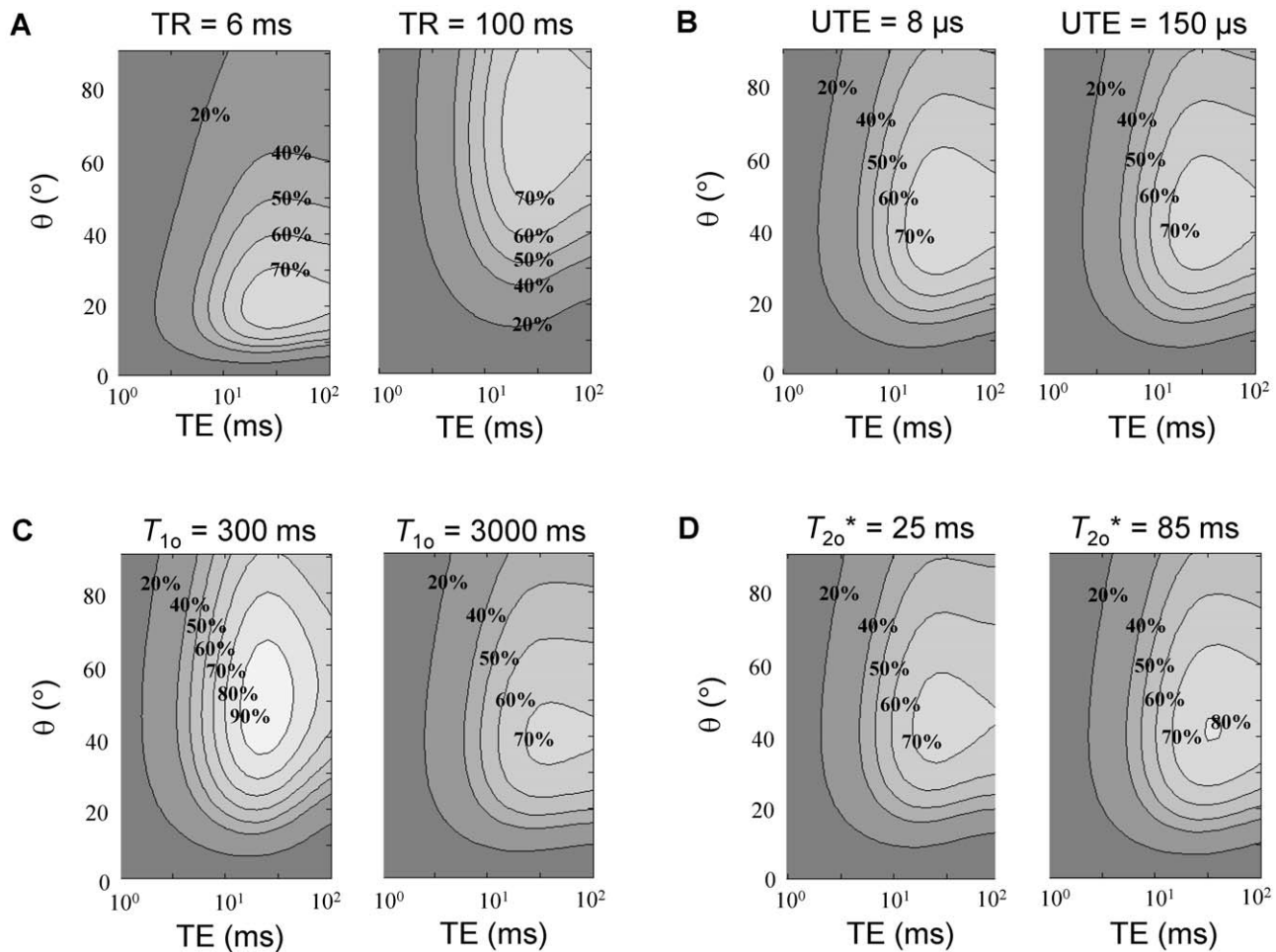


**Figure 2. Relative contrast of SubUTE for different sequence parameters and baseline tissue properties.** The relative contrast of SubUTE for different **A)** TR, **B)** UTE (i.e. shortest echo time), **C)** baseline tissue  $T_{10}$ , and **D)** baseline tissue  $T_{20}^*$  for a Mn concentration of 1.0 mM. Where parameters are held constant, the following values were used in addition to measured relaxivities of  $\text{MnCl}_2$ : TR = 30 ms, UTE = 90  $\mu\text{s}$ ,  $T_{10}$  = 1000 ms, and  $T_{20}^*$  = 47 ms. Relative contrast is expressed relative to the maximum contrast achieved on UTE. TR is seen to have the greatest influence on the optimal flip angle and TE (i.e. longer second echo). doi:10.1371/journal.pone.0058617.g002

echo (TSE) sequence: inversion times (TI) = [50, 100, 250, 500, 750, 1000, 1250, 1500, 2000, 2500] ms, TR = 3000 ms, TE = 18.5 ms, TSE factor = 4, 60 mm field-of-view (FOV), 3 mm slice thickness, and 0.5  $\times$  0.5 mm in-plane resolution.  $T_2$  were measured using a multi-echo spin-echo sequence: TR = 2000 ms, 32 echoes with TE = [7.63, 15.3, ..., 244] ms, 60 mm FOV, 3 mm slice thickness, and 0.5  $\times$  0.5 mm in-plane resolution. The relaxivity  $r_2$  was substituted for  $r_2^*$  in Eq. [2] as a first approximation for the phantom study. It is important to note that although this assumption is true for freely dispersed particles [13,14], we may expect  $r_2^*$  to be higher than  $r_2$  when Mn is clustered inside cells, based on evidence from the iron oxide literature that  $r_2^* \gg r_2$  upon cell internalization [15–17]. This point is discussed more fully in the Discussion.

The UTE sequence was run on the phantoms using a 3D steady-state gradient-echo sequence by varying TE (from 90  $\mu\text{s}$  to 10 ms) and  $\theta$  (10, 30, 50, and 70 $^\circ$ ) with TR fixed at 30 ms. As a preparation step, gradient channels were carefully calibrated to minimize off-resonance artefacts, and the tune delay of the coil was characterized for the shortest switching time. Multi-echo data with radial readout was then acquired with the following parameters: 60 mm cubic FOV, 3 mm slice thickness, and

0.5  $\times$  0.5 mm in-plane resolution, and one signal average. For comparison, a conventional 3D SPGR acquisition was also performed, using the same TR and  $\theta$  as in the UTE acquisition and setting TE = 2.83 ms (shortest).

### Breast Cancer Cell Studies

To investigate the value of UTE for positive-contrast imaging of Mn in biological systems, we labeled three different breast cancer cell lines with  $\text{MnCl}_2$ . The three breast cancers were 231/LM2-4, MDA-MB-231, and MCF-7. The first two are more aggressive than MCF-7, with 231//LM2-4 being a highly metastatic variant of MDA-MB-231 generated in the Kerbel lab [18]. The other two cell lines were obtained from ATCC (American Tissue Culture Collection, Manassas, VA, USA). These cell lines will be hereafter referred to as LM2, MDA, and MCF7, respectively. All cells were grown in 1640-RPMI medium (Sigma-Aldrich Canada Inc., Oakville, ON, Canada) supplemented with 10% fetal bovine serum and 0.5% penicillin streptomycin. Cells were harvested by washing 80–90% confluent flasks with PBS and adding 0.05% trypsin EDTA (Gibco, Carlsbad, CA, USA). Cells were incubated for 1 hour with medium containing different concentrations of  $\text{MnCl}_2$  while they were in the exponential growth phase, after

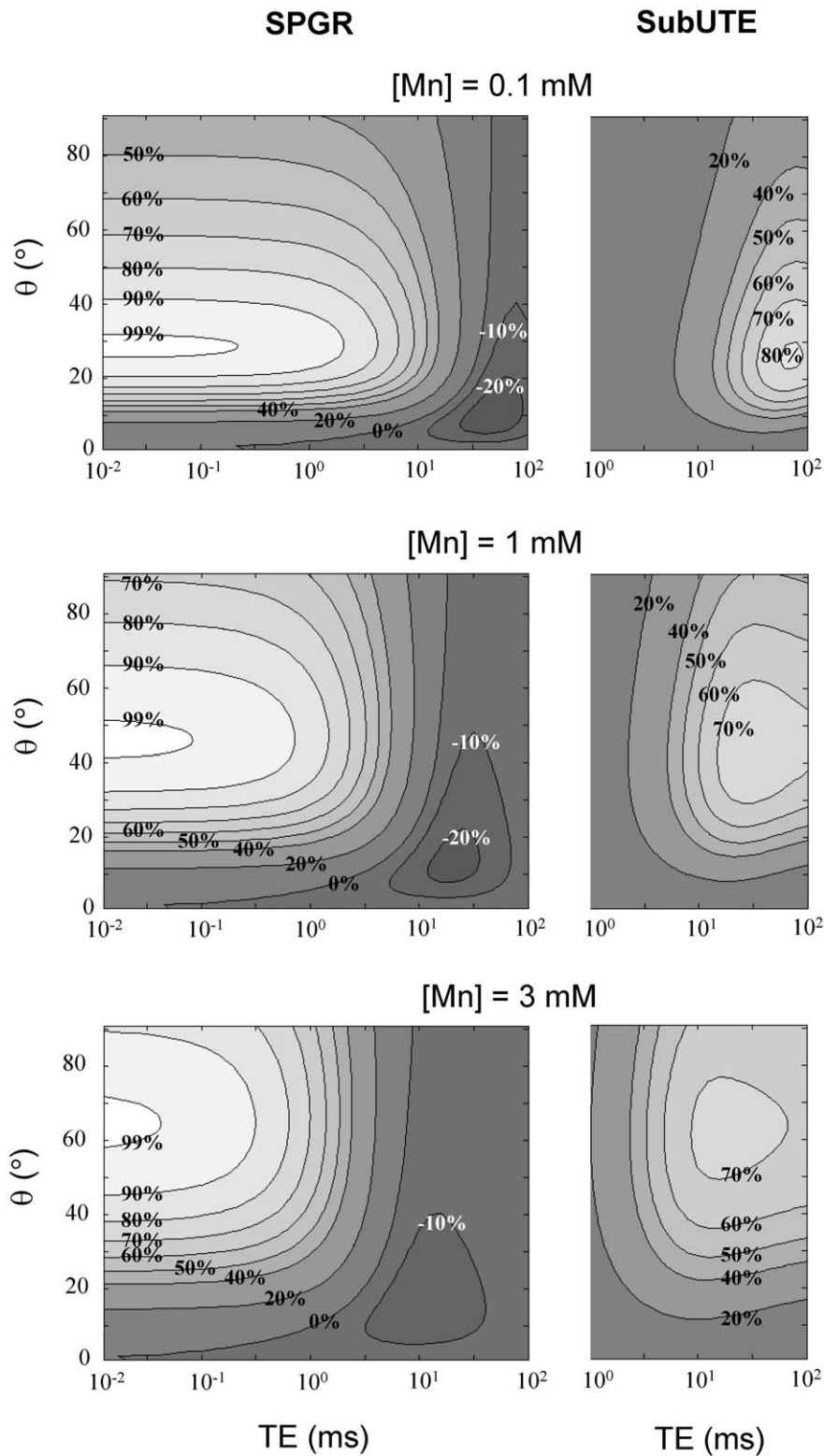


**Figure 3. Relative contrast of conventional SPGR (including UTE) and SubUTE for different  $\text{MnCl}_2$  concentrations.** Calculations were based on  $\text{TR} = 30$  ms, measured relaxivities of  $\text{MnCl}_2$ , and baseline tissue  $T_{10} = 1000$  ms and  $T_{20}^* = 47$  ms. To compare relative contrast of SPGR versus SubUTE, contrast isocontours are expressed relative to the maximum contrast achievable for each concentration. A  $\sqrt{2}$  noise penalty was accounted for in the difference signal of a SubUTE image. For SubUTE plots, the first echo was set to  $90 \mu\text{s}$  and the second longer echo is denoted as TE. It is seen that SPGR provides positive contrast at short TEs (including UTE) and negative contrast at longer TEs, whereas SubUTE provides strictly positive contrast.

doi:10.1371/journal.pone.0058617.g003

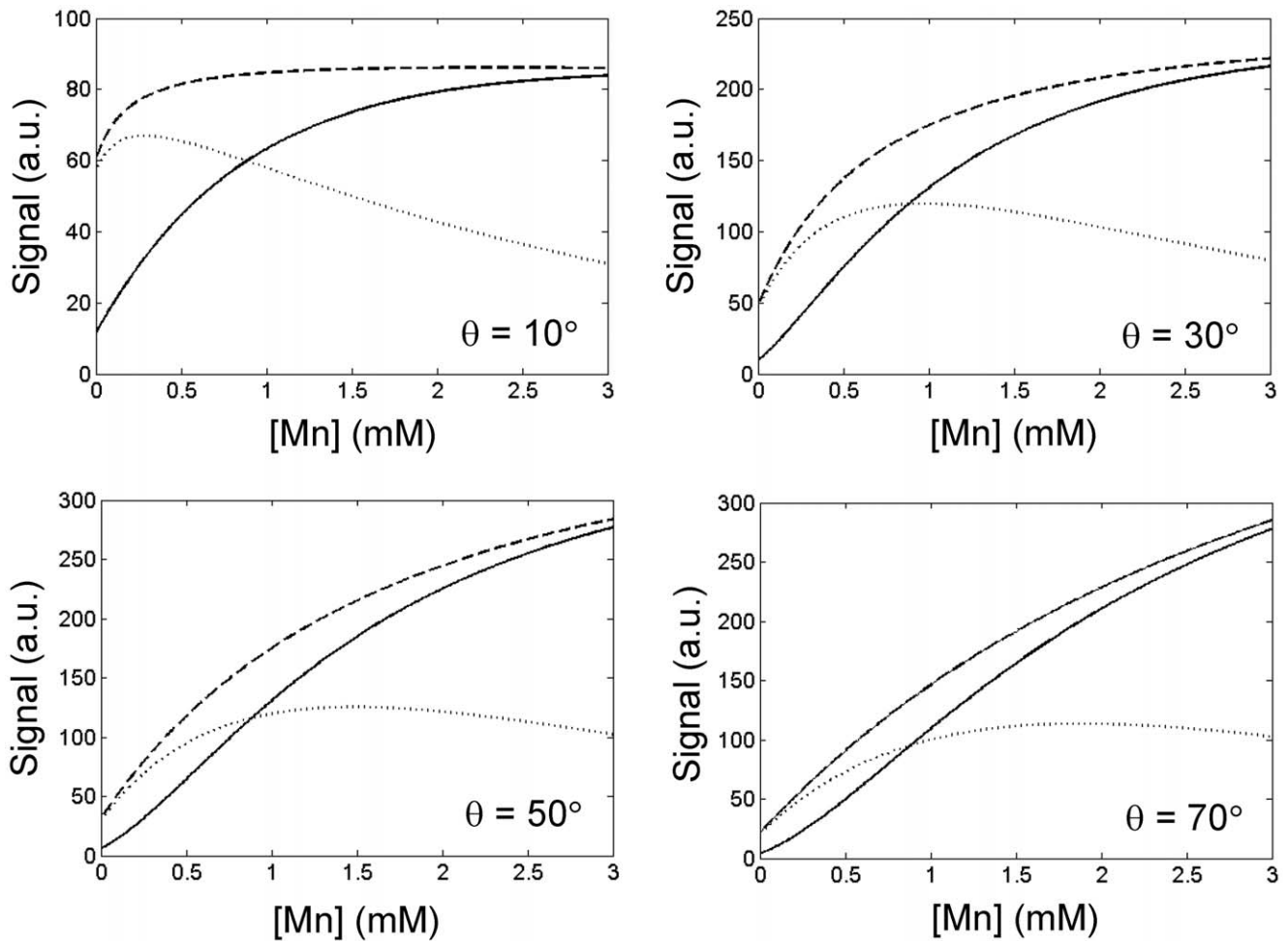


**Figure 4. Theoretical signal intensity curves for UTE, SubUTE, and conventional SPGR.** Signal intensity versus  $\text{MnCl}_2$  concentration for UTE (dashed line) with  $\text{TE} = 90 \mu\text{s}$ , SubUTE (solid line) with  $\text{TEs} = 90 \mu\text{s}$  and  $10 \text{ ms}$ , and conventional SPGR (dotted line) with  $\text{TE} = 2.83 \text{ ms}$ . Calculations were based on  $\text{TR} = 30 \text{ ms}$  and baseline tissue  $T_{10} = 1000 \text{ ms}$  and  $T_{20}^* = 47 \text{ ms}$ . A  $\sqrt{2}$  noise penalty was accounted for in the difference signal of a SubUTE image. It is seen that higher flip angles  $\theta$  provide greater positive contrast of high  $\text{MnCl}_2$  concentrations. doi:10.1371/journal.pone.0058617.g004

which they were rinsed with fresh medium and trypsinized as described above. Cell pellets were then prepared by centrifuge at  $440 \text{ g}$  for  $10 \text{ minutes}$  in the same borosilicate glass tubes used for phantom imaging. Immediately after, MRI was performed on breast cancer cell pellets on a  $3 \text{ Tesla}$  MRI scanner as described previously, using a range of  $\text{TEs}$  ( $90 \mu\text{s}$  to  $10 \text{ ms}$ ) and  $\theta$  ( $10, 30, 50,$  and  $70^\circ$ ).

#### Data Analysis

MRI data was transferred to an independent workstation for quantitative data analysis using in-house software developed in Matlab (v.7.8) (MathWorks, Natick, MA). To calculate the  $r_1$  and  $r_2$  relaxivities of  $\text{MnCl}_2$ , regions of interest (ROIs) were outlined in the center of each glass vial on each image and a signal intensity curve obtained at every pixel location within the ROI as a function of TI (for  $T_1$  measurement) or TE (for  $T_2$  measurement).  $T_1$  relaxation time was quantified on a pixel-wise basis by fitting signal intensity to the function  $A \times [1 - 2 \times \exp(-\text{TI}/T_1) + \exp(-\text{TR}/T_1)]$ , where  $A$  and  $T_1$  are free parameters.  $T_2$  relaxation time was quantified on a pixel-wise basis by fitting signal intensity to a mono-exponential decay function added to a constant offset to account for noise. The mean  $T_1$  and  $T_2$  within the ROI were calculated

along with the standard deviations. Relaxivities  $r_1$  and  $r_2$  were determined by linear regression analysis of the change in mean relaxation rates ( $1/T_1$  and  $1/T_2$ ) versus Mn concentration. For all phantom and breast cancer cell imaging data, comparisons amongst different sequences were made on a ROI basis.

#### Results

Measured relaxivity constants of aqueous  $\text{MnCl}_2$  at  $3 \text{ Tesla}$  are  $r_1 = 7.4 \text{ mM}^{-1}\text{s}^{-1}$  and  $r_2 = 117 \text{ mM}^{-1}\text{s}^{-1}$  (Figure 1). Note a much higher  $r_2/r_1$  ratio relative to Gd-based paramagnetic agents where the  $r_2/r_1$  ratio is roughly unity. The consequence of a large  $r_2/r_1$  ratio is the presence of  $T_2$ -related signal decay at higher contrast concentrations. While this is suboptimal for positive-contrast imaging and narrows the concentration range where enhancement can be reaped, it also provides an opportunity for additional contrast mechanisms offered by SubUTE imaging.

Simulations comparing the performance of conventional  $T_1$ -weighted SPGR versus UTE (i.e. SPGR with a very short TE) and SubUTE are shown in Figures 2, 3, 4. Figure 2 illustrates SubUTE contrast as a function of TR, UTE,  $T_{10}$  and  $T_{20}^*$ . Note that only TR has a significant effect on the position of the peak positive contrast. Figure 3 compares the relative contrast of conventional

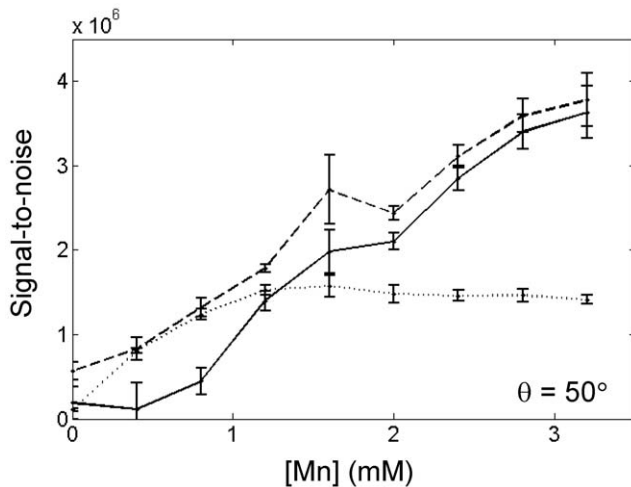


**Figure 5. Phantom signal-to-noise curves for UTE, SubUTE, and conventional SPGR.** Signal-to-noise in  $\text{MnCl}_2$  phantoms versus  $\text{MnCl}_2$  concentration for UTE (dashed line) with  $\text{TE} = 90 \mu\text{s}$ , SubUTE (solid line) with  $\text{TEs} = 90 \mu\text{s}$  and  $10 \text{ms}$ , and conventional SPGR (dotted line) with  $\text{TE} = 2.83 \text{ms}$ . Shown are mean values and standard deviations in each region-of-interest.  
doi:10.1371/journal.pone.0058617.g005

$T_1$ -weighted SPGR versus SubUTE generated by Mn at concentrations of 0.1, 1, and 3 mM as a function of TE and  $\theta$ . For illustrative purpose, a TR of 30 ms was chosen, as this value was consistent with the imaging requirements (i.e. imaging volume and slice thickness) of the in-vitro studies. In both Figures 2 and 3, contrast isocontours are expressed relative to the maximum contrast achievable for each concentration. Note also that although a range of TEs are shown up to 100 ms, the maximum relevant TE in any particular scenario cannot be larger than TR. The key purpose of Figure 3 is to show how to optimize contrast depending on the Mn range. In general, higher flip angles are necessary to maximize contrast at higher Mn concentrations, and, as shown in Figure 2, the optimal flip angle is tightly coupled to TR. The optimal TE for positive SubUTE contrast (i.e. the longer TE) and the optimal  $\theta$  are relatively independent of the tissue baseline  $T_{2o}^*$  and exhibit a dependence on  $T_{1o}$  only at very low contrast concentrations less than 0.1 mM (data not shown). Figure 4 provides another perspective for comparing the different sequences by showing signal intensity as a function of Mn concentration. As seen also in Figure 3, a higher flip angle provides more linear signal enhancement at higher concentrations. Most importantly, Figure 4 clearly shows that both UTE and SubUTE provide much more linear and sustained signal enhancement, even in the regime where signal plateau cannot be avoided on conventional  $T_1$ -weighted SPGR.

Phantom results confirmed theoretical predictions. Conventional  $T_1$ -weighted SPGR suffers from signal plateau and eventual signal decrease, whereas both UTE and SubUTE provide sustained and increasing positive contrast with higher Mn concentration. Figure 5 compares signal intensity on the different sequences for  $\theta = 50^\circ$ . The enhancement patterns are similar to simulation results.

Breast cancer cell imaging results are shown in Figure 6. Results are shown for  $\theta = 50^\circ$ , as this flip angle yielded the largest contrast changes across the different incubation concentrations. It is seen that the two aggressive cell lines, LM2 (top row) and MDA (middle row), take up much more Mn than MCF7 (bottom row) and, therefore, appear dark on  $T_2$ -weighted FSE and bright on

conventional  $T_1$ -weighted SPGR. Note that because we limited the contrast dosage to a maximum of 1.0 mM Mn for labelling cells, we have not entered the signal plateau regime. Nonetheless, it is clear that even though conventional  $T_1$ -weighted SPGR shows differences amongst the cancer cell lines, the UTE sequence provides slightly higher signal. By adding synergistic contrast mechanisms from  $T_2^*$  effects, the SubUTE sequence further emphasizes differences in Mn uptake between aggressive and less aggressive cancers. SubUTE provides the best distinction of aggressive breast cancers of all sequences, and only it provides simultaneous background tissue suppression.

## Discussion

The UTE sequence has been valuable for improving the visualization of normally dark-appearing iron oxide nanoparticles and tissue with short  $T_2$  and  $T_2^*$  (e.g. bone) by turning negative contrast into positive contrast. Although  $\text{MnCl}_2$  has  $T_1$  enhancing properties and does not share the same issues with negative contrast iron oxides on which UTE has been predominantly applied, the sensitivity and specificity of Mn-enhanced MRI can benefit from UTE imaging due to its characteristic high  $r_2/r_1$  ratio. In this study, we investigated through theoretical, phantom, and breast cancer cell studies the detection of Mn on UTE and SubUTE imaging. It is shown that UTE and SubUTE significantly broaden the range of Mn concentrations over which positive contrast is sustained and remains linearly increasing, compared to conventional SPGR that suffers from  $T_2^*$  effects at higher concentrations. This capability not only improves detection sensitivity but can potentially provide a means for quantifying contrast concentrations. It is also shown that because SubUTE is a subtraction technique, background tissue is effectively suppressed, which may enable more specific determination of Mn accumulation in a contrast-enhanced study without the use of a pre-contrast baseline image. Furthermore, since Mn has a relatively high  $r_2/r_1$  ratio, the SubUTE image can provide even greater contrast than UTE when  $T_1$  and  $T_2^*$  effects make comparable contributions, generally found at higher Mn concentrations; this is achieved by combining usually antagonistic  $T_1$  and  $T_2^*$  effects in a synergistic manner. Results in Mn-labeled breast cancer cells show that SubUTE achieves the best distinction of bright-appearing aggressive cancers from less aggressive cancers, which have similar contrast as background tissue.

Our theoretical study shows that optimal UTE and SubUTE contrast requires tuning the flip angle and TE to the range of Mn concentrations under consideration. For instance, higher concentrations of Mn translate to a lower  $T_1$ , which means that a higher flip angle is necessary to achieve maximum positive contrast. The second echo used to form the SubUTE image should ideally lie in the 10 ms range. Both the optimal flip angle and TE are determined primarily by Mn concentration and TR. Note in Figure 3 that the lower contrast in the SubUTE signal relative to the SPGR (or UTE) signal is partly due to a  $\sqrt{2}$  noise penalty in a SubUTE difference image and partly due to a strong  $T_1$  effect relative to  $T_2^*$ . Despite this lower sensitivity, SubUTE provides the greatest specificity of all sequences.

Phantom imaging confirmed theoretical predictions of signal plateau and eventual signal decrease on conventional SPGR, whereas UTE and SubUTE provided sustained positive contrast enhancement up to  $[\text{Mn}] = 3.2 \text{mM}$ , the maximum concentration tested. Optimal settings for flip angle and TE were similar to simulation results, with  $\theta = 50^\circ$  providing the optimum UTE and SubUTE contrasts over a wide range of concentrations.

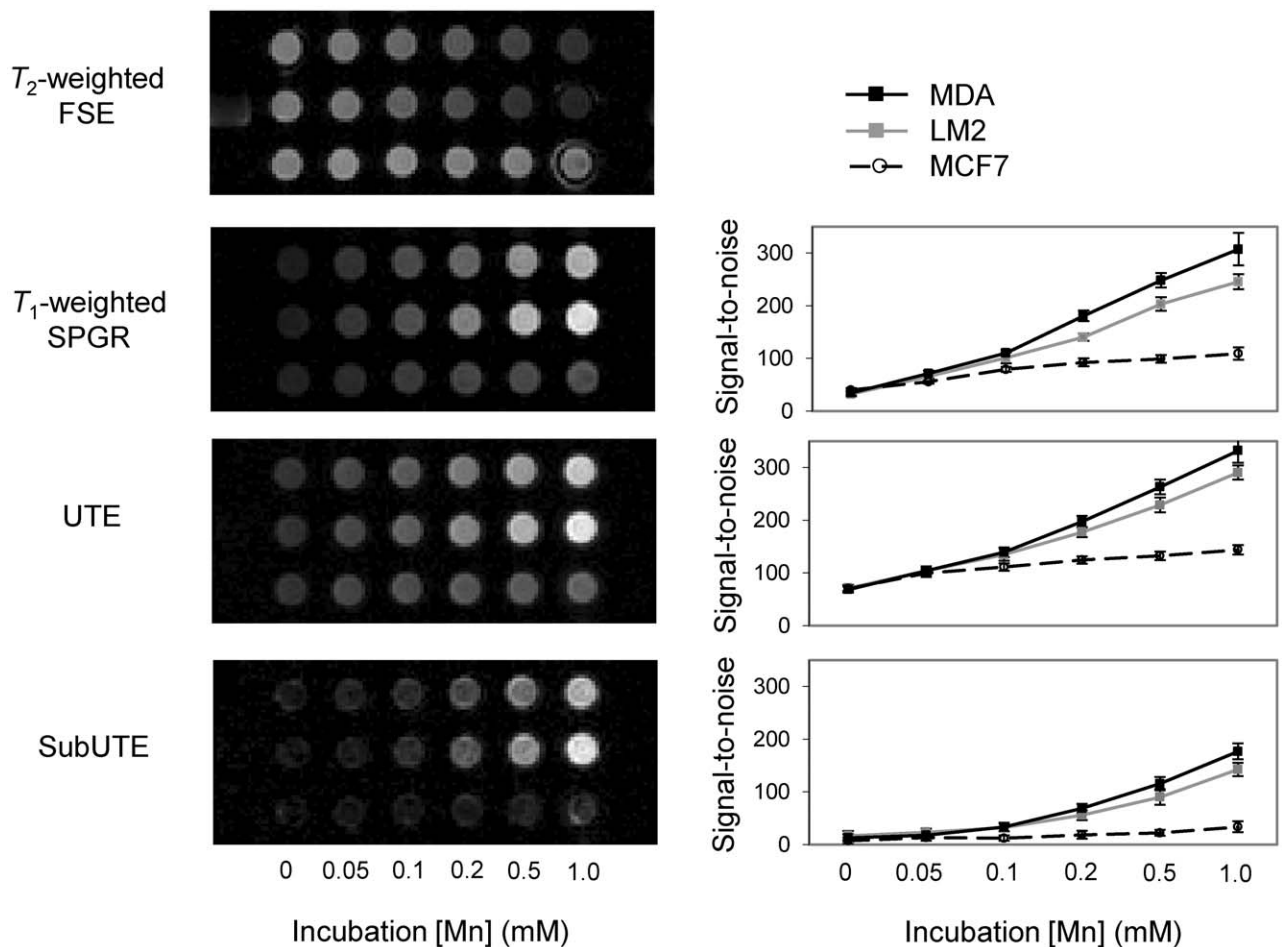


**Figure 6. Detection of aggressive breast cancer cells on UTE, SubUTE, and conventional SPGR.** Highly aggressive breast cancers LM2 (top row) and MDA (middle row) and less aggressive MCF7 (bottom row) incubated with  $\text{MnCl}_2$  at various concentrations are displayed as images (left column) and signal-to-noise (SNR) plots (right column). SNR plots present mean values and standard deviations in each region-of-interest. Cell uptake of Mn is seen as negative contrast on  $T_2$ -weighted FSE and positive contrast on other sequences. UTE ( $TE = 90 \mu\text{s}$ ) provides comparatively higher signal than conventional  $T_1$ -weighted SPGR. SubUTE ( $TE = 90 \mu\text{s}$  and 10 ms) suppresses unlabeled or background tissue and also suppresses low [Mn] accumulation, and provides the best contrast between aggressive and less aggressive breast cancers.  
doi:10.1371/journal.pone.0058617.g006

Breast cancer cell imaging also confirmed that UTE offered better sensitivity and SubUTE better specificity of Mn-enhanced aggressive cells than conventional SPGR. There are, however, a few distinct differences from the phantom studies. First, the Mn concentration range of the incubation medium was much lower (up to 1 mM) for the cell-labeling studies, as our aim was to use as low a dose as possible on cells. Over this concentration range, theory predicts that conventional SPGR has not yet entered the signal plateau regime seen in the phantom study, which our cell imaging results confirmed to be the case. However, theory also predicts an optimal flip angle less than  $50^\circ$  for the lower concentrations used to label cells. This discrepancy suggests a higher  $r_2^*$  relaxivity than predicted, which is potentially caused by the accumulation of Mn to a greater concentration in cells and/or the formation of Mn clusters. To fully explain and accurately predict contrast mechanisms in a cellular environment, we need to understand how Mn distributes within these cells. A better understanding of these effects is important for future in-vivo applications but is outside the scope of this article. Despite this discrepancy, it is clear that even in cells, the SubUTE approach is able to reap synergistic  $T_1$  and  $T_2^*$  effects at higher Mn concentrations and provide the best detection specificity.

The discrepancy in the cellular environment noted above highlights a fundamental challenge when simulating the in-vitro or in-vivo environment, namely, the deviation of contrast agent distribution from the ideal of free dispersion. We used a measurement of  $r_2$  as a first approximation to  $r_2^*$ , mainly because accurate measurement of  $r_2^*$  is challenging and prone to variations from a variety of sources. However, this assumption will likely not hold once Mn is internalized. As reported in the iron oxide literature,  $r_2^* \gg r_2$  when nanoparticles are compartmentalized in cells compared to free suspension [15–17]. Although Mn is not the same as iron oxides, we may postulate a similar phenomenon. That is, when Mn is internalized by cells, it does not distribute uniformly but, instead, accumulates in certain subcellular structures such as the mitochondria and forms clusters. As a result of compartmentalization,  $r_1$  will decrease due to limited water exchange and  $r_2^*$  will increase due to mesoscopic heterogeneities from bulk magnetic susceptibility effects. To optimize UTE and SubUTE imaging for cell studies, future work will need to investigate the distribution of Mn inside cells, how the distribution varies with different cell types, and the effect on  $r_2$  and  $r_2^*$  from varying Mn concentration and distribution.

Aside from the benefits of providing positive contrast and increased sensitivity under certain circumstances, perhaps the most practical advantage of SubUTE in vivo is background suppression, which effectively eliminates the need for a pre-contrast image. The convention of subtracting a pre-contrast baseline image from the contrast-enhanced image is cumbersome but is done to specifically locate areas of contrast agent accumulation. However, the baseline often cannot be perfectly co-registered, either because of patient movement or because contrast injection was done days earlier. With the SubUTE method, only one sequence is run and the contrast material can be localized wherever it has moved in the body and at any time, even days after contrast injection.

The use of Mn has gained renewed interest as an MRI contrast agent because of the potential to derived detailed physiological, biochemical, and molecular biological information [3]. In this study, we have presented a new application for Mn-enhanced MRI: assessing the aggressiveness of cancer cells. Our results demonstrate that our novel concept of using Mn to determine breast cancer aggressiveness is feasible and that the best distinction of aggressive versus less aggressive cells is achieved using SubUTE. Future studies will involve developing the proposed methodology in vivo, where safe contrast dosages and differences in the cellular environment (e.g. cell density) and deviation of relaxivities from the in-vitro scenario must be accounted for in optimizing UTE and SubUTE imaging. Beyond the demonstrated value of UTE for imaging cancer, it is our hope that with UTE as a new imaging capability for more sensitive and specific detection of Mn, many

more applications associated with Mn-enhanced MRI will be explored and developed to characterize biological systems.

## Conclusions

In this study, we have introduced a new application of UTE and SubUTE imaging for Mn-enhanced MRI. Although Mn is inherently a positive-contrast  $T_1$  agent, UTE and SubUTE improve detection sensitivity over conventional SPGR, and they enable sustained and linear positive contrast enhancement over a wide range of Mn concentrations, even at high concentrations where signal would normally plateau or decrease. The SubUTE sequence provides additional specificity of Mn accumulation by eliminating background tissue and even increased sensitivity under certain circumstances by combining usually antagonistic  $T_1$  and  $T_2^*$  effects. Contrast localization on SubUTE does not require a pre-contrast baseline image, which is a significant advantage in any contrast-enhanced examination.

## Acknowledgments

We thank Melanie S. Kotys-Traugher from Philips Healthcare, Cleveland, Ohio, USA, for implementing the UTE sequence.

## Author Contributions

Cell preparation: JN. Image acquisition: JN HLC. Conceived and designed the experiments: HLC. Performed the experiments: JN HLC. Analyzed the data: HLC. Contributed reagents/materials/analysis tools: JN HLC. Wrote the paper: HLC.

## References

- Lauterbur PC, Dias MH, Rudin AM (1978) In: Dutton PL, Leigh JS, Scarpa A, editors. *Frontiers of Biological Energetics*. New York: Academic Press. 752–759.
- Mendonca-Dias MH, Gaggelli E, Lauterbur PC (1983) Paramagnetic contrast agents in nuclear magnetic resonance medical imaging. *Semin Nucl Med* 13: 364–376.
- Koretsky AP, Silva AC (2004) Manganese-enhanced magnetic resonance imaging (MEMRI). *NMR Biomed* 17: 527–531.
- Braga HJ, Choti MA, Lee VS, Paulson EK, Siegelman ES, et al. (2002) Liver lesions: manganese-enhanced MR and dual-phase helical CT for preoperative detection and characterization comparison with receiver operating characteristic analysis. *Radiology* 223: 525–531.
- Lin YJ, Koretsky AP (1997) Manganese ion enhances T1-weighted MRI during brain activation: an approach to direct imaging of brain function. *Magn Reson Med* 38: 378–388.
- Brurak H, Skoglund T, Berg K, Skarra S, Karlsson JO, et al. (1999) Myocardial manganese elevation and proton relaxivity enhancement with manganese dipyriddyoxyl diphosphate. Ex vivo assessments in normally perfused and ischemic guinea pig hearts. *NMR Biomed* 12: 364–372.
- Brismar TB, Kartalis N, Kylander C, Albiin N (2012) MRI of colorectal cancer liver metastases: comparison of orally administered manganese with intravenously administered gadobenate dimeglumine. *Eur Radiol* 22: 633–641.
- Baio G, Fabbi M, Emionite L, Cilli M, Salvi S, et al. (2012) In vivo imaging of human breast cancer mouse model with high level expression of calcium sensing receptor at 3T. *Eur Radiol* 22: 551–558.
- Bergin CJ, Pauly JM, Macovski A (1991) Lung parenchyma: projection reconstruction MR imaging. *Radiology* 179: 777–781.
- Girard OM, Du J, Agemy L, Sugahara KN, Kotamraju VR, et al. (2011) Optimization of iron oxide nanoparticle detection using ultrashort echo time pulse sequences: comparison of T1, T2\*, and synergistic T1–T2\* contrast mechanisms. *Magn Reson Med* 65: 1649–1660.
- Zhang L, Zhong X, Wang L, Chen H, Wang YA, et al. (2011) T(1)-weighted ultrashort echo time method for positive contrast imaging of magnetic nanoparticles and cancer cells bound with the targeted nanoparticles. *J Magn Reson Imaging* 33: 194–202.
- Crowe LA, Ris F, Nelles-Vallespin S, Speier P, Masson S, et al. (2011) A novel method for quantitative monitoring of transplanted islets of langerhans by positive contrast magnetic resonance imaging. *Am J Transplant* 11: 1158–1168.
- Bulte JW, Brooks RA, Moskowitz BM, Bryant LH, Jr., Frank JA (1999) Relaxometry and magnetometry of the MR contrast agent MION-46L. *Magn Reson Med* 42: 379–384.
- Weissleder R, Cheng HC, Bogdanova A, Bogdanov A, Jr. (1997) Magnetically labeled cells can be detected by MR imaging. *J Magn Reson Imaging* 7: 258–263.
- Bowen CV, Zhang X, Saab G, Gareau PJ, Rutt BK (2002) Application of the static dephasing regime theory to superparamagnetic iron-oxide loaded cells. *Magn Reson Med* 48: 52–61.
- Girard OM, Ramirez R, McCarty S, Mattrey RF (2012) Toward absolute quantification of iron oxide nanoparticles as well as cell internalized fraction using multiparametric MRI. *Contrast Media Mol Imaging* 7: 411–417.
- Kotek G, van Tiel ST, Wielopolski PA, Houston GC, Krestin GP, et al. (2012) Cell quantification: evolution of compartmentalization and distribution of iron-oxide particles and labeled cells. *Contrast Media Mol Imaging* 7: 195–203.
- Munoz R, Man S, Shaked Y, Lee CR, Wong J, et al. (2006) Highly efficacious nontoxic preclinical treatment for advanced metastatic breast cancer using combination oral UFT-cyclophosphamide metronomic chemotherapy. *Cancer Res* 66: 3386–3391.